ISSN 1069-3513, Izvestiya, Physics of the Solid Earth, 2023, Vol. 59, No. 4, pp. 531–543. © Pleiades Publishing, Ltd., 2023.
Russian Text © The Author(s), 2023, published in Fizika Zemli, 2023, No. 4, pp. 39–52.

Electrical Resistivity of ε-Fe at High Pressures of Stepwise Shock Compression

A. M. Molodets[a], * and A. A. Golyshev[a]

[a] *Institute of Problems of Chemical Physics, Russian Academy of Sciences, Chernogolovka, 142432 Russia*

**e-mail: molodets@icp.ac.ru*

Received July 10, 2022; revised October 23, 2022; accepted November 23, 2022

Abstract—In situ electrical resistance measurements are performed on samples of iron with a hexagonal close–packed lattice (ε-Fe), compressed and heated by stepwise shock loading. Equations of state for ε-Fe are constructed. The obtained experimental results are mathematically simulated in the hydrocode based on the developed equations of state. The modeling results are used to reconstruct the volume temperature dependence of the ε-Fe electrical resistivity at pressures of ≈20–70 GPa and temperatures of ≈750–950 K. The volume–temperature dependence of the ε-Fe thermal conductivity coefficient is calculated according to the Wiedemann–Franz law. The results obtained for the electrical and thermal conductivity of shock compressed and heated ε-Fe are compared with literature experimental and theoretical data for iron and silicon iron.

Keywords: iron, electrical conductivity, thermal conductivity, high pressures, equations of state, phase diagram, shock waves

DOI: 10.1134/S1069351323040080

INTRODUCTION

Seismological observations and thermophysical properties of geophysical materials at high pressures and temperatures (*P*-*T*) suggest that the Earth's inner cores are mainly composed of an iron alloy containing ≈85% iron, ≈5% nickel and ≈10% some light elements—silicon, carbon, etc. Therefore, understanding the thermal state of the core, as well as the generation and evolution of the Earth's magnetic field, largely depends on the reliability of information about the electrical properties of iron compositions, and primarily on pure iron (see (Zharkov, 2012; Hirose et al., 2021; Zhang et al., 2022) and references therein).

The values of pressure and temperature of the deep layers of the Earth are hundreds of gigapascals and thousands of degrees, and on the phase diagram of iron they are located in the region of existence of the compressed and heated ε-Fe phase of iron with a hexagonal close-packed (*hcp*) lattice. In this regard, an extensive scientific literature is devoted to the study of various properties of compressed and heated ε-Fe iron, including its electrical properties, at high pressures and temperatures.

The dependence of the electrical resistivity of ε-Fe iron $\rho = \rho(P, T)$ on pressure P and temperature T in the pressure range up to 200 GPa and temperatures up to 3000 K was measured under both hydrostatic compression and shock-wave loading. Most measurements of the electrical conductivity of heated ε-Fe iron were performed under static conditions of hydrostatic compression of diamond anvils with external laser heating (see (Seagle et al., 2013; Gomi et al., 2013; Zhang et al., 2020; Zhang et al., 2022) and references therein).

The electrical resistance in situ of shock-compressed and shock-heated ε-Fe iron samples was studied in (Keeler and Mitchel 1969; Bi et al., 2002). Shock wave data can complement hydrostatic data for a number of positions. First, at microsecond times of shock-wave loading, parasitic effects associated with possible (see, for example, (Basu et al., 2020; Yang et al., 2022)) chemical reactions of hot iron with the surrounding materials of the measuring cells of static presses decrease. In addition, in the case of plane one-dimensional shock-wave compression, the change in the geometrical dimensions of the samples, which is necessary for the transition to the specific values of electrical resistance, is reliably taken into account. Finally, at the same temperatures and pressures, a difference in the electrical properties of a sample heated by shock compression and a compressed sample statically heated cannot be excluded.

Measurements of the electrical resistance of samples under plane shock wave loading are most often performed using foil samples surrounded by an insulating material with a different impedance. Therefore, the shock-wave compression of the samples occurs in the so-called stepped shock compression mode, in which the Lagrangian particle of the material is continuously compressed by successive shock waves (see

(Nabatov et al., 1979; Adadurov, 1986) and their references).

The use of stepped shock compression, similar to gradual dynamic compression (ramp compression (Remington et al., 2015)) provides a choice of more wide regions of the phase diagram of iron in the vicinity of the single compression state along the material's Hugoniot. Along with this, the design capabilities of the stepwise shock compression scheme make it possible to purposefully vary the parameters of the loading regime within the required limits. Thus, in a thin sample at a certain ratio of the sample thickness and dynamic impedance of the materials of the experimental assembly, a stepped-cyclic compression mode is realized with a high-frequency pressure component at each step (Molodets et al., 2021). Within the framework of this scheme, it is possible to measure the electrical resistance of a sample in an extended range of pressures and temperatures in a single shock-wave experiment, which makes it preferable in the tasks of detailing the electrical properties of materials under conditions of strong dynamic compression.

The physical interpretation of the experimental results on the electrical conductivity of shock-compressed samples requires knowledge of the equation of state and the possibility of modeling the electrophysical and thermodynamic properties of the material under study under the conditions of the experiment. Modern computers and computational methods make it possible to calculate the thermodynamic and electrophysical properties of compressed iron from first principles (see the paper by (Vocadlo, 2007) and the references therein). However, the results of complex first–principles calculations are in the form of digital arrays that are separated from the initial physical assumptions by non–trivial numerical procedures. In this case, the semiempirical description of the experimental data remains relevant, since it can be easily used in hydrocodes and, at the same time, provide an accurate description of the ε-Fe properties. In such a situation, the best option is a semi-empirical description of the electrophysical and thermodynamic properties of iron (see, for example, (Seagle et al., 2013; Bi et al., 2002)), which turns out to be convenient for use in hydrocodes and at the same time provides an accurate description of the properties ε-iron due to a set of free parameters in physically justified mathematical relationships

This paper presents the results of measuring the electrical resistance of ε-Fe samples under step-cyclic shock compressions to pressures of 70 GPa and a modified description of the obtained experimental results based on semiempirical models of the electrical and thermophysical behavior of iron from (Seagle et al., 2013; Molodets and Golyshev, 2021).

SAMPLES, STEP-CYCLIC SHOCK LOADING AND REGISTRATION OF ELECTRICAL RESISTANCE OF SHOCK COMPRESSED IRON SAMPLES

The test samples were made from ARMCO iron foil. According to GOST 11036-75, ARMCO iron contains impurities in mass percentages of no more than 0.035% C, 0.3% Mn, 0.3% Si, 0.020% P, 0.030% S, 0.3% Cu. The measured electrical resistivity and density of the samples were 10.05(5) μΩ cm and 7.85(3) g/cm^3, respectively, which are characteristic of the α-Fe phase (body-centered cubic (bcc) iron) at room temperature and atmospheric pressure.

A schematic diagram of the stepwise shock load generator used is shown in Fig. 1a according to (Molodets et al., 2021). Here, flat metal impactor *1* collides with layered target *2–4*, consisting of two steel plates *2* and *4* and insulating (Teflon) layer *3* sandwiched between them. After the collision, a single shock wave impulse is formed in plate *2*, the front of which takes on a stepwise shape in layer *3* in the form of pressure increases P_1, P_2, P_3 (see Fig. 1b). This transformation is caused by the reverberation of the compression wave in "soft" Teflon *3* between two "hard" steel plates *2* and *4*.

Ribbon–shaped iron sample *5* and ribbon–shaped manganin gauge *6* (photos of the manganin gauge and the sample are shown in Fig. 2a) are located in the center of layer *3*. The successive arrival of each of the stages P_1, P_2, P_3 at gauges *5* and *6* also induces reverberations of attenuated compression and decompression waves in them. This process is shown as a high frequency cyclic pressure component at the fronts of the stages P_1, P_2, P_3 in Fig. 1b. The stepwise shock compression phase ends when the maximum pressure P_{max} is reached at the moment t_{max}. Then the pressure gradually decreases down to zero, mainly due to the arrival of the decompression wave from the free surface of thin plate *4*. It should be noted that the half–period of the cyclic component τ_0 at the fronts of the stages P_1, P_2, P_3 is of the order of $\tau_0 \sim h_0/C_0$, where h_0 is the thickness of the gauge, C_0 is the speed of sound of the gauge material. So, with $h_0 \approx 0.05$ mm and $C_0 \approx 5$ mm/μs, which are typical of metal, $\tau_0 \approx 0.01$ μs.

The stepwise shock load generator thus produces a specific loading condition in iron sample *5*, consisting of a "stepwise–cyclic" phase of compression to pressures P_{max}, followed by a phase of gradual pressure reduction.

The electrical resistance of ε-Fe sample *5* is measured if P_{max} exceeds $P_{0\varepsilon}$ and $P_{\varepsilon\alpha}$, where $P_{0\varepsilon}$ is the pressure at the end of the direct polymorphic transition and $P_{0\varepsilon}$ is the pressure at the beginning of the inverse polymorphic transition of α-Fe (iron with a body–centered cubic (bcc) lattice) into ε-Fe. Indeed, in this case, in the process of shock wave compressions of the

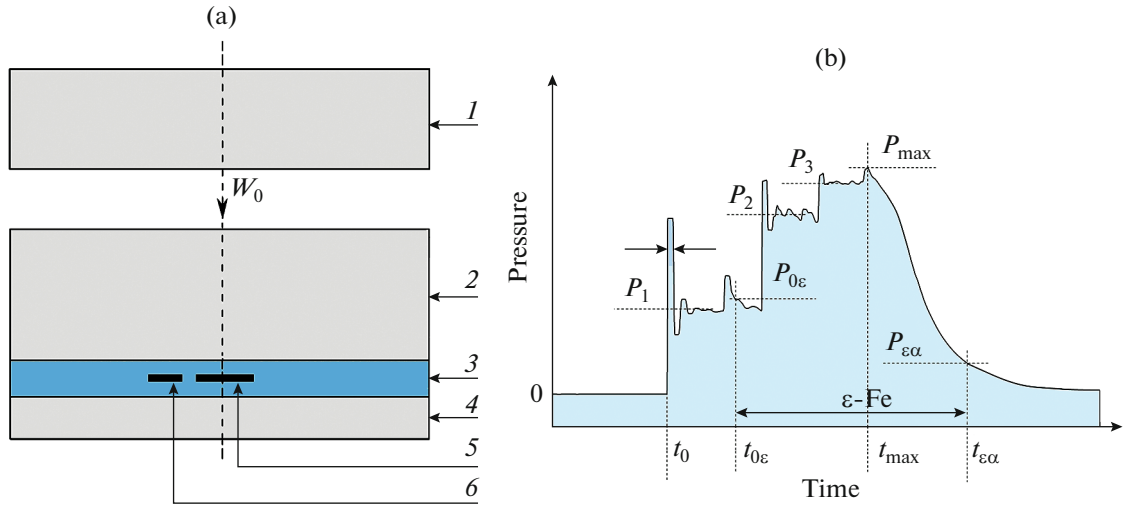

Fig. 1. The stepwise-cyclic shock load generator (a), and the profile (time dependence) of the pressure in the studied sample when measuring its electrical resistance (b); (a): *1*—a disc–shaped steel (12X18H10T stainless steel) impactor with a thickness of 3.5 mm, accelerated by explosion products to a velocity of W_0 = 2.6(1) km/s; *2*—a stainless steel plate with a thickness of 3.45(1) mm; *3*—insulating TVC material (Teflon films bonded with vacuum grease) with a thickness of h_0 = 2. 45(1) mm; *4*—a thin stainless steel plate with a thickness of 1.85 mm; *5*—the iron sample under study; *6*—the sensing element of the manganin pressure sensor (*5* and *6* are located in one plane); (b)—the symbols are explained in the text.

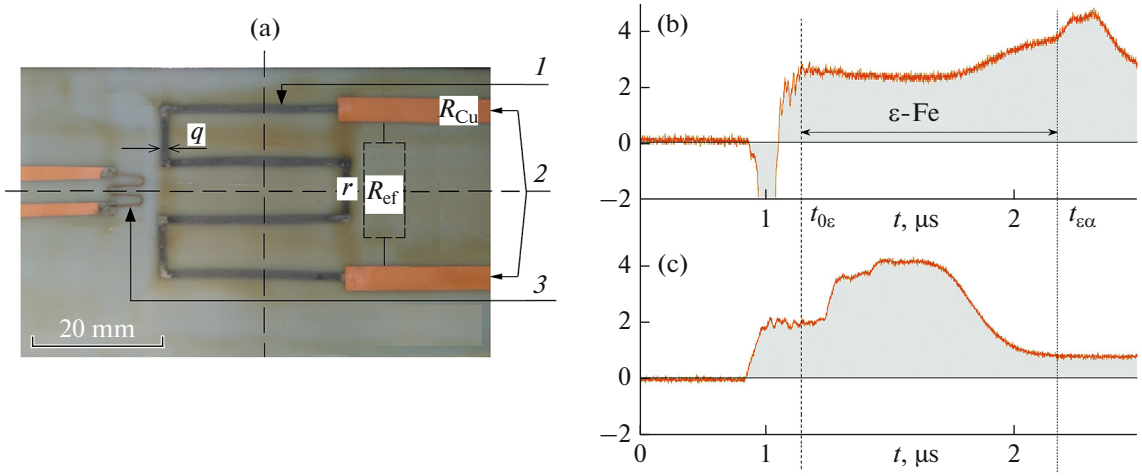

Fig. 2. The sensing elements of ribbon–shaped gauges (a) and their primary signals (b), (c): (a) the load cell of the magnetic transformation gauge; *1*—the sensing element of the gauge used with a thickness of h_0 = 60 μm and a width of q = 1 mm; *2*—copper current leads with a thickness of 30 μm; *3*—the manganin pressure gauge with a thickness of 60 μm; (b) and (c) the primary signals of gauges *1* and *3*, respectively, in the form of electric voltage profiles $U(t)$.

iron sample, we can determine the interval $t_{0\varepsilon} < t < t_{\varepsilon\alpha}$ of the ε-Fe existence, as shown schematically in Fig. 1b.

The interval $t_{0\varepsilon} < t < t_{\varepsilon\alpha}$ was determined and the profile of the iron sample's electrical resistance $R(t)$ was measured by means of the load cell from the study by (Molodets et al., 2021), a photo of which is shown in Fig. 2a, as mentioned above. Here, in the process of stepwise shock loading, independent currents of known amplitude are passed through iron sample *1* and manganin gauge *3* to determine the change in their electrical resistance $R(t)$ from the measured voltage drop $U(t)$.

The result of the single experiment is shown in Figs. 2b and 2c as the primary $U(t)$ (t—time) profiles from gauge *1* and *3*, respectively. According to the paper by (Molodets et al., 2021), the oscillogram of gauge *1* in Fig. 2b contains signals of polymorphic transformation. These signals appear as a negative impulse in the region $t_{0\varepsilon}$ and as a positive deflection at the moment $t_{\varepsilon a}$. It should be noted that oscillogram *1* in Fig. 2b is one of three oscillograms that match

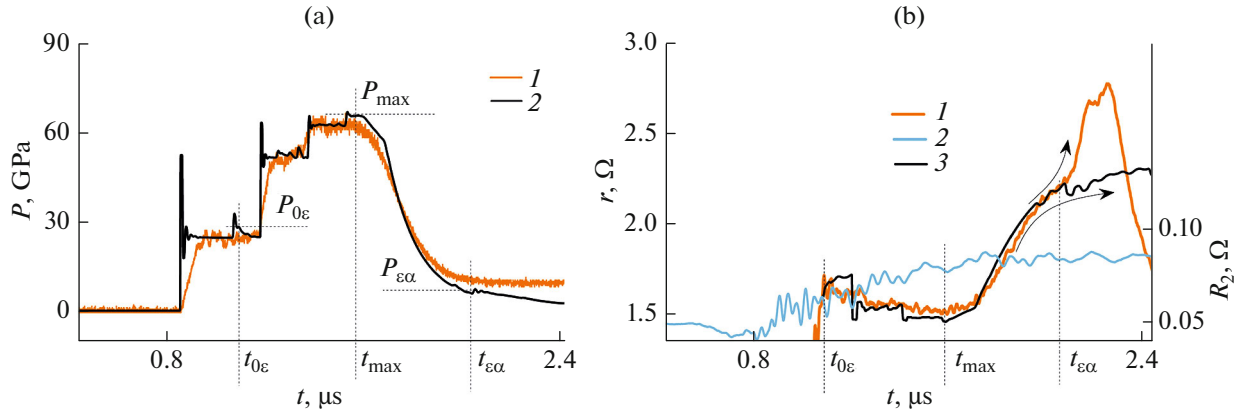

Fig. 3. The experimental and model profiles of pressure and electrical resistance. (a): *1*—the pressure profile obtained from processing the readings of the manganin gauge, *2*— the calculated pressure profile in the iron sample (the meaning of the symbols $t_{0\varepsilon}$, t_{max}, $t_{\varepsilon\alpha}$, $P_{0\varepsilon}$ P_{max} $P_{\varepsilon\alpha}$ is the same as in Fig. 1b); (b): *1*—the corrected electrical resistance profile $r = r(t)$ of the studied ε-Fe sample; *2*— the electrical resistance profile of gauge *1–2* in Fig. 2a, in which iron sample *1* was replaced with its copper equivalent; *3*—the calculated electrical resistance profile $r = r(t)$ in the ε-Fe sample (left ordinate r for *1* and *3*, right R_2—for *2*).

within 3% in three identical experiments. Thus, it is possible to find the time interval $t_{0\varepsilon} < t < t_{\varepsilon\alpha}$ of ε-Fe existence in the oscillograms of Fig. 2b to determine the primary profile $R_1 = R_1(t)$ of the electrical resistance of the ε-Fe sample in the shock wave experiments performed.

Manganin gauge *3* is of the same thickness and in the same plane as gauge *1*. Therefore, its electrical resistance changes at the same time as the electrical resistance of the sample changes, and the primary signal $U(t)$ of the manganin gauge in Fig. 2c, recalculated into pressure, practically coincides with the amplitudes of the shock compression and decompression steps in sample *1*. In Fig. 3a, *1* indicates the $P(t)$ profile in a typical experiment.

However, it should be noted that experimental profile *1* lacks the high–frequency cyclic component in the pressure steps. There are two possible reasons for this discrepancy. The first reason is the limited frequency characteristics of the manganin technique, which does not allow the detection of signals with a duration of $\tau_0 \approx 0.01$ μs. At the same time, the primary signal of the manganin gauge may also be reduced by the component of the manganin electrical resistivity dependence on temperature. Therefore, experimental pressure graph *1* in Fig. 3a is used only to estimate the pressure at the plateau of the $P(t)$ profile steps and also to mark the time when the shock wave disturbances arrive at the gauge plane.

As for the iron sample, the pressure profile in the sample was further calculated in the hydrocode based on the developed equations of state presented below. The calculated profile of pressure in the iron sample is shown in graph *2* in Fig. 3a, where $P_{max} = 67$ GPa. As can be seen, calculated profile *2* contains all the features of the schematic pressure profile of Fig. 1b.

Thus, the applied technique allows us to determine the time interval of ε-Fe existence to study its electrophysical properties under high pressures of the stepwise–cyclic compression phase up to the pressures P_{max} and subsequent gradual decompression.

CONSIDERATION OF COMPLICATING EFFECTS IN THE MEASUREMENT OF THE ELECTRICAL RESISTANCE OF SHOCK COMPRESSED IRON SAMPLES

It should be noted that the technique described above has a number of features that make it difficult to analyze the measurement results. Indeed, at high shock compression pressures, the insulator may lose its insulating properties and shunt the sample to some extent. One way to reduce the shunting of the iron sample was applied in the study by (Bi et al., 2002), where a resistant corundum insulator was used. In our study, the electrical resistance r of the iron sample was preliminarily shunted by the insulating so-called TVC medium. Secondly, the electrical resistance of the sample measured with the two–point technique contains a "parasitic" electrical resistance of the copper current leads, R_{Cu}.

These two complications were accounted for as follows. In the experiment with the iron sample, the primary profile $R_1 = R_1(t)$, obtained by the recalculation of the $U(t)$ oscillogram, was equated to the value $R_1 = 2R_{Cu} + rR_{ef}/(r + R_{ef})$. The meaning of the summands and factors in this expression is explained in Fig. 2a: R_{Cu} is the "parasitic" electrical resistance of one copper current leads, r is the electrical resistance of the iron sample, R_{ef} is the effective electrical resistance of the insulating TVC medium connected in parallel to r. We then used the results of an identical experiment in which the iron sample was replaced by a copper ribbon

with the electrical resistance r_c. In the copper ribbon experiment, the measured profile $R_2 = R_2(t)$ was equated to $R_2 = 2R_{Cu} + r_cR_{ef}/(r_c + R_{ef})$. After excluding the electrical resistance of the copper current leads R_{Cu} from the two expressions for R_1 and R_2, we can write:

$$r = R_{ef}\left(\Delta R + \frac{r_cR_{ef}}{r_c + R_{ef}}\right)\left(R_{ef} - \left(\Delta R + \frac{r_cR_{ef}}{r_c + R_{ef}}\right)\right)^{-1},$$

where $\Delta R = R_1\text{-}R_2$.

It should be noted that the resulting expression for r can be simplified. Indeed, according to the paper by (Golyshev and Molodets, 2013), the dependence of the effective electrical resistance of the insulating TVC medium R_{ef} on the pressure P can be presented in the form $R_{ef} = 4.38P^{47.07/P}$, where R_{ef} and P are expressed in Ω and GPa, respectively. At the maximum pressures of ≈ 70 GPa achieved in the conducted experiments, the effective electrical resistance of the insulation was $R_{ef} \approx 75$ Ω. At the same time, the experiments with the iron sample and with the copper ribbon show that $R_2 \ll R_1$ and $R_2 < 0.1$ Ω (see profile *2* in Fig. 3b). Since it is obvious that $r_c < R_2$, in general $r_c \ll R_{ef}$, $r_c \ll \Delta R$ and hence,

$$r \cong \frac{R_{ef}\Delta R}{R_{ef} - \Delta R}. \quad (1)$$

The electrical resistance profile $r = r(t)$ of the studied ε-Fe sample adjusted according to (1) is shown by graph *1* in Fig. 3b.

It should also be noted that the paper by (Molodets et al., 2021) uses a capacitor of $C = 1000$ μF as the current source, which is discharged through the resistance $R \approx 100$ Ω. Thus, an alternating current of the order of $\omega \sim 2\pi/(RC)$ is actually flowing through the sample. Let us estimate the skin effect for this frequency in the conducted experiments. Since the thickness $h_0 = 60$ μm of iron sample *1* is much less than its width $q = 1$ mm (see Fig. 2a), the sample can be considered to be a plate and the well–known formula for the current penetration depth $d = 0.5(\omega\mu\mu_0/\rho)^{-1/2}$ in a flat layer can be applied to it. Here, μ is the magnetic permeability of the sample substance, μ_0 is the magnetic constant, and ρ is the electrical resistivity. Using the characteristic values $\mu \approx 5000$ and $\rho \approx 10$ μΩ cm for iron, we obtain the estimate $d \approx 700$ μm. Thus, the conducted experiments had the ratio $d \gg h_0$, which means that the skin effect is small with almost constant current density across the cross–section of the studied iron sample.

Finally, let us evaluate one more factor of possible distortions of the results in the conducted experiments on measuring the electrical conductivity of a sample surrounded by Teflon insulation. Generally speaking, the destruction of the shock-compressed Teflon insulator with the release of fluorine and the subsequent formation of an iron fluoride film on the surface of the iron sample are not excluded. However, the estimate of the film thickness δ by the formula $\delta^2 \sim Dt_d$ with the diffusion coefficient $D \sim 10^{-12}$ m^2/s for microsecond times t_d of the shock wave experiment is thousandths of a micron. The smallness of the value of δ in comparison with the thickness h_0 of the samples under study makes it possible to neglect the corresponding possible contribution to the measured electrical resistance $r = r(t)$.

As noted in the introduction, the physical interpretation of the experimental results in the form of electrical resistance profiles $r = r(t)$ (1) requires knowledge of the equation of state for the ε-Fe phase of iron and the possibility of modeling the electrophysical and thermodynamic properties of the material under study under the conditions of the experiment. The equations of state for the ε-Fe phase of iron and modeling of the obtained experimental data are presented in the following two sections of the article.

EQUATIONS OF STATE FOR ε-Fe AT HIGH PRESSURES AND TEMPERATURES

The thermodynamic state of ε-Fe was calculated from the equation of state (EOS) for α-Fe from the paper by (Molodets and Golyshev, 2021) and the EOS for ε-Fe constructed specifically for this study. The equations of state were found by means of partial derivatives of the semiempirical expression for the Helmholtz free energy of an isotropic solid compressed from all sides $F = F(V,T)$. The thermal equation of state (the dependence of pressure P on volume and temperature T) is determined by the partial derivative of the Helmholtz free energy with respect to volume $P = P(V,T) = -\partial F/\partial V$. The caloric equation of state (dependence of internal energy E on volume and temperature) is determined by the partial derivative of the Helmholtz free energy with respect to temperature $E = F - T(\partial F/\partial T)$. The technique of constructing the EOSs and the formulas of the basic expressions used for the Helmholtz free energy in the form

$$F = 3R\left[\frac{\Theta}{2} + T\ln\left(1 - \exp\left(-\frac{\Theta}{2}\right)\right)\right] + E_x + E_m, \quad (2)$$

where R is the specific gas constant, the key function $\Theta = \Theta(V)$ is the Einstein characteristic temperature, and the key function $E_x = E_x(V)$ is the potential energy, are similar to those in the paper by (Molodets et al., 2017) (See also the paper by (Molodets, 2022)), E_m is the difference between potential energies of α-Fe and ε-Fe iron phases. Thus, $\Theta = \Theta(V)$ is expressed as follows:

$$\Theta = \Theta_0\left(\frac{\upsilon_0 - V}{\upsilon_0 - V_0}\right)^2\left(\frac{V_0}{V}\right)^{2/3}. \quad (3)$$

In (3), the parameter υ_0, which has the meaning of the characteristic volume, is determined as follows:

Table 1. Parameters for the Helmholtz free energy (2) for α-Fe (Molodets and Golyshev, 2021) and for ε-Fe

Phase	V_0, cm^3/mol	Θ_0, K	υ_0, cm^3/mol	υ_x, cm^3/mol	C_1, GPa	C_2, GPa	C_3, kJ/g	E_m, kJ/g
α-Fe	7.093	279.8	21.092	21.02	−144.5188	2971.046	−572.4635	0.0
ε-Fe	6.76[b]	262.1	17.949	13.858	−724.8081	15070.4575	−1876.6370	0.8127

$$\upsilon_0 = V_0\left(\frac{3\gamma_0 + 4}{3\gamma_0 - 2}\right), \quad (4)$$

where $\gamma_0 = \gamma_0(V_0, T_0)$ is the Grüneisen parameter for the initial specific volume V_0, the initial room temperature $T_0 = 298.15$ K, and the initial atmospheric pressure P_0. Accordingly, the parameter Θ_0 represents the initial value of the characteristic temperature $\Theta_0 = \Theta(V_0)$.

$E_x = E_x(V)$ is expressed as follows:

$$E_x = -\nu_x\left(C_1 H_x + C_2 x\right) + C_3, \quad (5)$$

$$H_x = 9x^{\frac{1}{3}}\left(\frac{1}{10}x^{-1} + 2 + \frac{3}{2}x - \frac{1}{7}x^2 + \frac{1}{70}x^3\right), \quad x = \frac{V}{\upsilon_x}. \quad (6)$$

Table 1 shows the Helmholtz free energy parameters (2) for α-Fe and for ε-Fe used in this study.

The adequacy of the EOSs for α-Fe was discussed in the paper by (Molodets and Golyshev, 2021). Figure 4 shows calculations *1* and *4* for ε-Fe obtained from (2) and the data in Table 1. As can be seen, our calculations for ε-Fe are also in satisfactory agreement with the experimental data, both for static compression (Mao et al., 1990; Dewaele et al., 2006) and for shock wave compression (Brown et al., 2000).

MODELING OF THE THERMODYNAMIC STATE AND THE VOLUME–TEMPERATURE DEPENDENCE OF THE ε-Fe ELECTRICAL RESISTIVITY IN THE CONDUCTED EXPERIMENTS

The developed EOSs for iron phases make it possible to calculate the thermodynamic properties of iron in extensive regions of its phase diagram and to simulate the thermodynamic state of iron samples in the conducted experiments. Thus, Fig. 5 shows equilibrium line *1* between α-Fe and ε-Fe, calculated from (2) and the data in Table 1, and temperature *2* along the single shock compression adiabatic of ε-Fe.

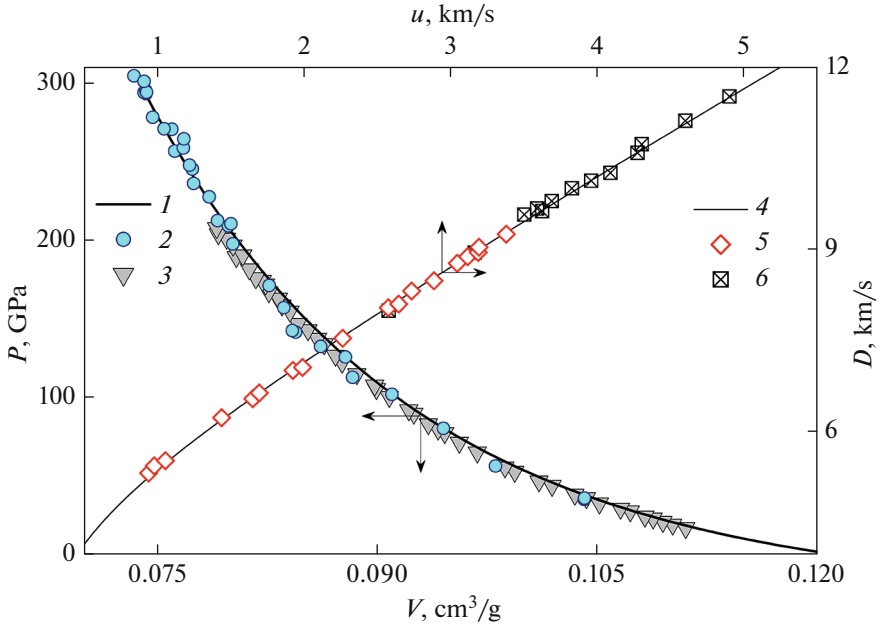

Fig. 4. The calculated and experimental results of ε-Fe shock and static compression: *1*—the calculated room temperature isotherm in the pressure *P*—volume *V* coordinates; *2* and *3*—the experimental room temperature isotherms from the papers by (Mao et al., 1990; Dewaele et al., 2006), respectively; *4*—the calculated single shock Hugoniot in the shock wave velocity *D*—mass velocity *u* coordinates; *5*—the refined experimental data from explosion experiments (Brown et al., 2000); *6*—the experimental Hugoniot determined with a two–stage light–gas gun according to the paper by (Brown et al., 2000).

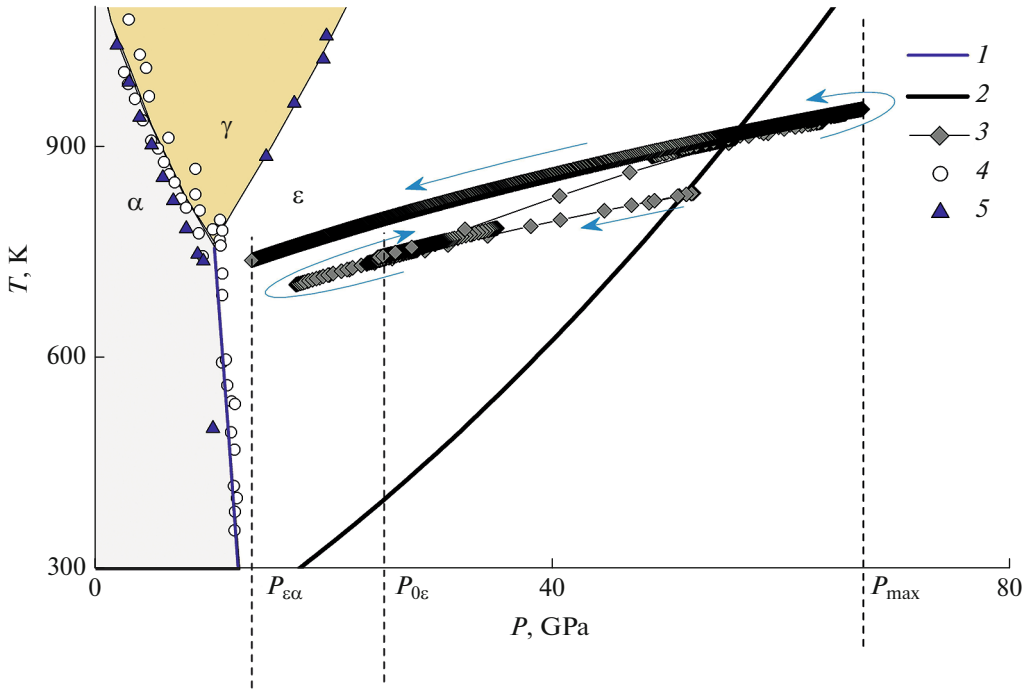

Fig. 5. The studied region of the iron phase diagram in the pressure P—temperature T coordinates: *1*—the author's calculation of the equilibrium line between α-Fe and ε-Fe; *2*—the calculated temperature along the ε-Fe Hugoniot; *3*—the calculated phase trajectory of the ε-Fe stepwise-cyclic shock loading in the conducted experiments (the arrows indicate the sequence of the states in time); *4* and *5*—the literature experimental points of the equilibrium line between the iron phases taken from the papers by (Johnson, 1962; Kerley, 1993); the meaning of the symbols $P_{\varepsilon\alpha}$, $P_{0\varepsilon}$ and P_{max} is the same as in Fig. 3a.

The thermodynamic state of the iron samples was simulated in the conducted experiments with the STAG software (Kim and Molodets, 2016). This software can calculate wave interactions and thermodynamic states in the form of pressure $P(t)$, temperature $T(t)$, and volume $V(t)$ profiles for selected Lagrangian particles of the impactor and each layer of multilayered targets in Fig. 1a under one–dimensional shock loading. The STAG software does not allow heat exchange between target layers. The pressure $P(t)$, temperature $T(t)$ and volume $V(t)$ profiles were calculated in the STAG software from the author's equations of state for the materials of the experimental setup. Since the width of the iron sample $q \approx 1$ mm is an order of magnitude greater than its thickness of $h_0 \approx 0.05$ mm, in the hydrocode the sample was modeled by a plate with an initial thickness of h_0. The EOSs for iron were used as given above, the EOS for stainless steel was used as given in the paper by (Molodets, 2015), and the EOS for Teflon was used as given in the paper by (Molodets et al., 2013).

Let us focus here on whether the calculation of the temperature of the shock compressed sample surrounded by the shock heated insulator is acceptable. Figure 6a shows model profile *1* of the temperature $T(t)$ for the center of the ε-Fe sample. This figure also shows the calculated profiles of temperatures *2* and *3* in the "soft" insulator before and after the sample, respectively. As can be seen, the "soft" insulator heats up significantly more than the "hard" sample during shock compression. In other words, in the conducted experiments, the iron sample plate is sandwiched between two hot layers of insulating Teflon. Therefore, it is obvious that neglecting the heat exchange between the sample and the insulator is acceptable only if the time of the experiment is much shorter than the time τ needed for the iron sample plate to heat up to the temperature T_τ of the surrounding insulator. Let us calculate τ using the well–known formula for estimating τ by order of magnitude:

$$\tau \sim \frac{\delta^2}{a}. \qquad (7)$$

In (7), δ is half the thickness of the plate, $a = Vk/C_P$ is the thermal conductivity coefficient, where: V is the specific volume; k is the thermal conductivity coefficient; C_P is the isobaric heat capacity. Let us make an estimate from (7), taking into account the changes in plate thickness $\delta = 0.5h_0(V/V_0)$, specific volume $V = V(t_{max})$ and thermophysical properties of iron under the conditions of the experiment conducted at pressure values $P_{max} = 67$ GPa at time t_{max}. We find the corresponding values to be $V = 5.691$ cm^3/mol (see profile *1* in Fig. 6b), $V_{0\alpha} = 7.093$ cm^3/mol, $\delta = 24$ μm, $C_P = 25.81$ J/mol K. The value T_τ is assumed to be $T_\tau =$

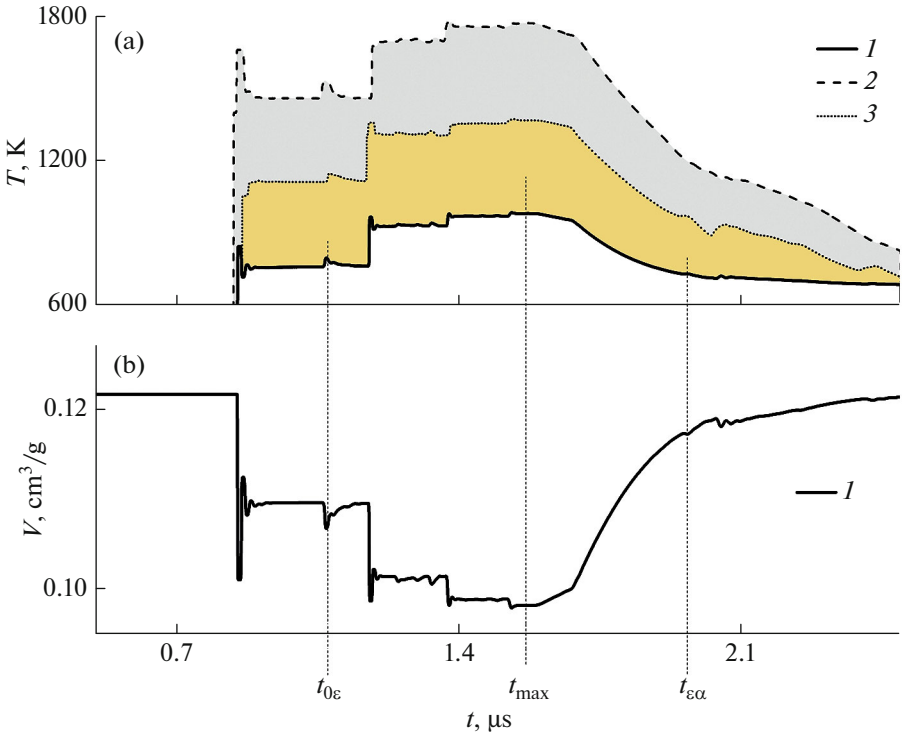

Fig. 6. The model temperature and specific volume profiles under stepwise-cyclic shock wave loading of the ε-Fe sample and the Teflon surrounding material. (a) The temperature profiles: *1*—the temperature profile in the center of the ε-Fe sample with a thickness of 60 μm; *2*—the temperature profile in the Teflon film in front of the sample at a distance of 30 μm from the sample surface; *3*—the temperature profile in the Teflon film behind the sample at a distance of 30 μm from the sample surface; (b) the specific volume profile in the center of the ε-Fe sample with a thickness of 60 μm.

$T_\tau(t_{max}) = 1375$ K, which is the temperature of the Teflon behind the sample (see profile *3* in Fig. 6a). The value k is assumed to be the thermal conductivity coefficient of ε-Fe heated to 1375 K at a pressure of 53 GPa as in the paper by (Hasegawa, 2019), which is equal to $k = 47$ W/(mK). The above values give the estimate $\tau \sim 56$ μs, which is much longer than the time of the experiment, which is ≈1 μs. Thus, the relationship between the sample heating time and the time of the experiment allows us to neglect the heat exchange between the sample and the insulator and to use the resulting temperature profiles when analyzing and modeling the experimental data obtained for ε-Fe under stepwise shock compression.

So Figure 6a shows model profile *1* of the temperature $T(t)$ for the center of the ε-Fe sample. An example of the calculated profile of the pressure $P(t)$ of ε-Fe is shown above in Fig. 3a. Excluding time from the $P(t)$ and $T(t)$ profiles will give the phase trajectory of the sample in the pressure–temperature coordinates, shown in Fig. 5 by graph *3*, which outlines the region of the iron phase diagram in which the ε-Fe electrical resistivity under stepwise shock compression has been measured. This region can be characterized by pressures of ≈20–70 GPa and temperatures of ≈750–950 K. As can be seen in Fig. 3, phase trajectory of stepwise shock compression *3* is significantly different from single shock compression adiabatic of ε-Fe *2*.

The calculated temperature $T = T(t)$ and volume $V = V(t)$ profiles were also used to simulate the profile of the sample's electrical resistance $R = R(t)$ along the phase trajectory of stepwise shock compression according to the formula:

$$R = R_{0\alpha}\left(\frac{\rho(T,V)}{\rho_{0\alpha}}\right)\left(\frac{V_{0\alpha}}{V}\right). \quad (8)$$

In (8), the index "0α" means that the property corresponds to α-Fe at room temperature and atmospheric pressure. The sample's initial resistance $R_{0\alpha}$ and its electrical resistivity $\rho_{0\alpha}$ were measured before the experiment and were $R_{0\alpha} = 0.23(1)$ Ω and $\rho_{0\alpha} = 10.1(8)$ μΩcm, respectively. The last factor in parentheses (8) accounts for the change in thickness of the sample during one–dimensional compression. The initial specific volume of α-Fe $V_{0\alpha}$ was equal to $V_{0\alpha} = 7.093$ cm³/mol.

The function $\rho = \rho(T,V)$ in (8) is a defining relation for the volume–temperature dependence of the ε-Fe specific electrical resistivity in the form of a modified function of volume and temperature as in the paper by (Seagle et al., 2013):

$$\rho = \rho_0 \left(\frac{T}{T_0}\right)^{\alpha} \left(\frac{V}{V_0}\right)^{n/3} \left(\frac{\upsilon_0 - V)}{\upsilon_0 - V_0}\right)^{-2n}. \quad (9)$$

In (9), the meaning of the key parameters ρ_0, α, n is the same as in the prototype of (Seagle et al., 2013), and the parameters υ_0 and V_0 are additional parameters as modified in the paper by (Molodets and Golyshev, 2021). According to the paper by (Molodets and Golyshev, 2021), the parameters υ_0 and V_0 are also the parameters that define the volume dependence of the characteristic temperature in formula (3). For ε-Fe, the parameters υ_0 and V_0 were taken from Table 1. The value of the initial resistivity ρ_0 at room temperature and atmospheric pressure is assumed to be $\rho_0 = 51.0$ μΩ cm for metastable ε-Fe as in the paper by (Gomi et al., 2013).

It should also be noted that in the time interval $t_{max} < t < t_{\varepsilon\alpha}$ (see Fig. 6), we can approximate the temperature–volume relationship $T = T(V)$ by the monotonic quadratic function $T(V) = A + BV + CV^2$ and determine the coefficients A, B, C in the standard way. For example, for the specific model profiles in Fig. 6, $A = 3383.3$ K, $B = -626.16$ K/(cm^3/g), $C = 33.21$ K/(cm^3/g)^2. This possibility and equation (8) allow us to write the model relation for the sample's electrical resistance profile $R = R(t)$ (8) as

$$R = R_0 \left(\frac{\rho_0}{\rho_{0\alpha}}\right)\left(\frac{T(V)}{T_0}\right)^{\alpha} \left(\frac{V}{V_0}\right)^{n/3} \left(\frac{\upsilon_0 - V)}{\upsilon_0 - V_0}\right)^{-2n} \left(\frac{V_{0\alpha}}{V}\right). \quad (10)$$

Thus, in the time interval $t_{max} < t < t_{\varepsilon\alpha}$, model relation (10) for the volume–temperature dependence of the sample's electrical resistance $R = R(t)$ along the phase trajectory of stepwise shock compression can be represented by a semiempirical volume function containing one predetermined parameter $\rho_0 = 51.0$ μΩ cm and two adjustable parameters: α, and n. The parameters α, and n are found by the least squares method based on the best fit between model profile (10) and the experimental profile $R = R(t)$. Figure 3b shows a satisfactory fit between experimental *1* and model *3* profiles of the sample's electrical resistance during unloading in the time interval $t_{max} < t < t_{\varepsilon\alpha}$. In this case, the values of the key parameters α, n and the coefficient of determination R^2 were as follows: $\alpha = 0.77(1)$, $n = 3.25(10)$ and $R^2 = 0.977$.

Thus, the developed equations of state for ε-Fe together with the defining relation for the volume–temperature dependence of the electrical resistivity make it possible to model the electrophysical shock wave experiment and to determine the "temperature" α and "volume" n parameters characterizing the volume–temperature dependence $\rho = \rho(T,V)$ of the ε–Fe electrical resistivity during its stepwise shock loading in the range of pressures ~20–70 GPa and temperatures ~750–950 K. Consequently, defining relation (9) with the found coefficients represents experimentally calculated data on the electrophysical properties of ε-Fe under stepwise shock wave loading conditions.

DISCUSSION

It should be noted that the values $\rho_0 = 51.0$ μΩ cm, $\alpha = 0.77(1)$, $n = 3.25(10)$ for ε-Fe found from experimental data in the decompression region give acceptable results in the compression region of ε-Fe as well. Indeed, experimental *1* and model *3* profiles in Fig. 3b agree with each other not only in the time interval $t_{max} < t < t_{\varepsilon\alpha}$, when the pressure decreases, but also in the time interval $t_{0\varepsilon} < t < t_{max}$, when the pressure increases from $P_{0\varepsilon}$ to P_{max}. This indicates that the model equation (9) with the found parameters α and n for the volume–temperature dependence of the ε-Fe specific electrical conductivity is adequate to the experimental shock wave data in the studied range of pressures ~20–70 GPa and temperatures ~750–950 K both during compression and during decompression.

Let us compare the electrophysical properties of ε-Fe iron under conditions of shock compression and under conditions of high static pressures. To do this, we use the equation of state developed above and calculate the isotherms and isobars of the volume-temperature dependence (9) for iron ε-*Fe*.

In Fig. 7a the number *1* denotes isotherm (9) at a temperature of 300 K in the pressure–electrical resistivity coordinates up to 80 GPa. Figure 7a also shows the model room isotherm *2* from (Seagle et al., 2013) for experimental points *3*. As can be seen, plot *1* is located significantly higher than plot *2*. The formal reason for this difference is mainly as follows. Despite the fact that the meaning of the main parameters ρ_0, α, n of the model relations for $\rho = \rho(T,V)$ in (Seagle et al., 2013) and in formula (9) is the same, the procedure for finding these parameters for (9) and in (Seagle et al., 2013) are different. In (Seagle et al., 2013) it was assumed in advance that $\alpha = \text{const} = 1$, while ρ_0 and n were adjustable. As noted above, in our work, the parameter $\rho_0 = \text{const} = 51.0$ μΩ cm was considered constant, and α and n were adjustable. We preferred our own version due to the fact that the value $\rho_0 = 51.0$ μΩ cm has an experimental justification for ε-Fe iron at zero pressure (see (Gomi et al., 2013)).

Figure 7a also shows hydrostatic experimental room isotherms *4* (Zhang et al., 2020) and *5* (Gomi et al., 2013). As can be seen, in the pressure range of 20–80 GPa, our room isotherm *1* exceeds the literature data *3, 4, 5* by 10–20 μΩ cm. Obviously, this difference can be partly interpreted on the basis of generally accepted ideas. Indeed, as is well known, shock waves generate a significant density of defects in the crystal lattice, which leads to an increase in the electrical resistivity of a shock-compressed polycrystal.

Let us discuss the relationship between the obtained results and literature data at high pressures and temperatures of shock-wave and hydrostatic com-

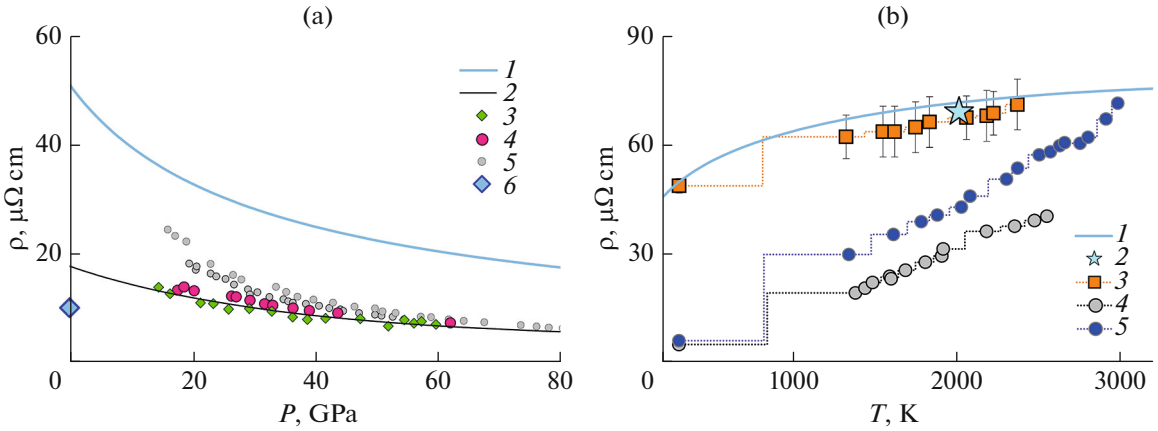

Fig. 7. Dependence of electrical resistivity ρ of compressed and heated ε-Fe iron on pressure *P* and temperature *T*. (a): *1*—room temperature isotherm (9); *2*—fitting room temperature isotherm from (Seagle et al., 2013), *3*, *4*, *5*—experimental results, respectively, from (Seagle et al., 2013; Zhang et al., 2020; Gomi et al., 2013), *6*—initial electrical resistivity of the investigated samples of iron ARMCO at room temperature and atmospheric pressure; (b) isobars at a pressure of 105 GPa: *1*—calculated ε-Fe iron isobar (9), *2*—shock-wave experiment (Bi et al., 2002), *3*—experimental isobar of the ε-Fe iron alloy with 4.3% Si from (Zhang et al., 2022), *4* and *5*—are experimental ε-Fe iron isobars from (Ohta et al., 2016; Zhang et al., 2020), dotted lines are the horizontal spline over points without scatter.

pression along high-pressure isobars. Graph *1* in Fig. 7b shows the calculated isobar of relation (9) for iron ε-Fe at a pressure of 105 GPa in the temperature range of 250–3000 K. It is difficult to compare it with shock wave data from (Keeler and Mitchel, 1969) since the work does not indicate the values of temperatures and volumes. In contrast, in (Bi et al., 2002) for two states (101 GPa; 2010 K) and (208 GPa; 5220 K) of shock-compressed ε-Fe iron, the electrical resistivity values are 68.9 and 130.7 μΩ cm respectively. The first point (Bi et al., 2002) is indicated in Fig. 7b as number *2*. As can be seen, results *1* and *2* practically coincide. The second point differs from the calculations according to (9) by 20%. Thus, in general, the agreement between our results and the results of (Bi et al., 2002) can be considered satisfactory. Note for what follows that results *1* and *2* in Figs. 7b, coinciding with each other, they also coincide with isobar *3* of the heated iron-silicon alloy Fe4.3%Si.

Figure 7b shows the static experimental ε-Fe iron *4* (Ohta et al., 2016) and *5* (Zhang et al., 2020). As for the isotherms, our isobar *1* is located significantly higher than the experimental isobars ε-Fe of iron—here the differences reach 30 μΩ cm. This discrepancy between the obtained and published hydrostatic data could be attributed to unnoticed parasitic effects of the shock wave technique used. At the same time, it seems that the list of possible methodological errors (shunting, thermal conductivity, skin effect, reaction of iron with a heated insulator) has been exhausted above and does not support this explanation. Therefore, it is possible that the mutual arrangement of all isotherms in Fig. 7a and isobars in Fig. 7b is due to the fact that shock-compressed ε-Fe iron is in a certain state in which its electrical properties differ from statically compressed pure ε-Fe iron and approach electrophysical properties of compressed and heated Fe4.3%Si iron-silicon alloy. However, it is obvious that this explanation is just a working hypothesis that requires additional argumentation and verification.

Let us now estimate the volume-temperature dependence of the thermal conductivity coefficient of shock-compressed ε-Fe iron. Let us again use relation (9) in conjunction with the equation of state developed above and compare the calculated values of the thermophysical properties of shock-compressed ε-*Fe* iron with the literature data at high static pressures. To do this, let us calculate the baric dependence of the ε-Fe thermal conductivity $k = k(V,T)$ along the room isotherm using the Wiedemann–Franz law

$$k = L\frac{T}{\rho(V,T)}, \qquad (11)$$

where $L = 2.45 \times 10^{-8}$ WΩ/K^2 is the Lorentz constant, $\rho(V,T)$ is the volume–temperature dependence of the ε-Fe electrical resistivity (9) with the coefficients ρ_0, α and n determined above. In Fig. 8, *1* indicates graph (11) obtained at $T = \text{const} = 300$ K. In the same figure, diamonds *2* show the experimental values of the thermal conductivity coefficient of polycrystalline ε-Fe, copied from Fig. 10 of the paper by (Ohta et al., 2018). As can be seen, graph *1* is in satisfactory agreement with the static experiment, passing through midpoint *3* of the data from the paper by (Ohta et al., 2018).

Let us now consider the isobar of the thermal conductivity coefficient at high pressure. Figure 9 shows isobar *1*, as graph (11) at a pressure of 53 GPa against the experimental points obtained by static compression in the paper by (Hasegawa et al., 2019) in a temperature range of 1200–1500 K at the same pressure.

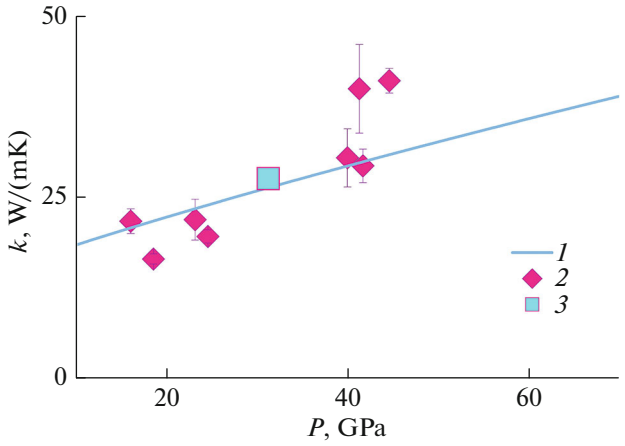

Fig. 8. Dependence of the heat transfer coefficient k (11) on the pressure P for ε-Fe at constant temperature $T = 300$ K: *1*—room temperature isotherm (11); *2*—the experimental results from the paper by (Ohta et al., 2018); *3*—the midpoint of the data from the paper by (Ohta et al., 2018).

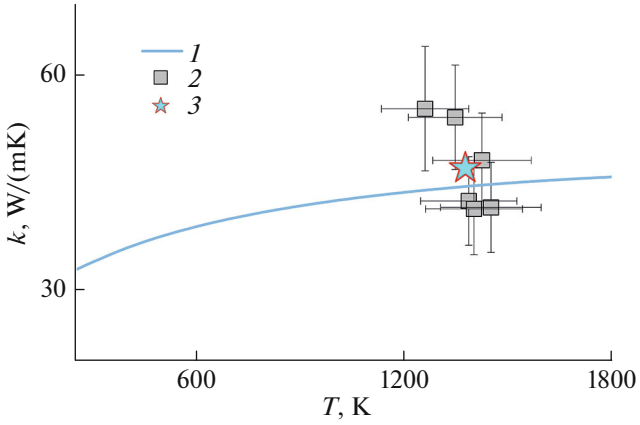

Fig. 9. Dependence of the thermal conductivity coefficient k (11) on the temperature T for ε-Fe at constant pressure $P = 53$ GPa: *1*—isobar (11); *2*—the experimental results from the paper by (Hasegawa et al., 2019) in a range of 1200–1500 K; *3*—the midpoint of the data from the paper by (Hasegawa et al., 2019).

Here, our shock wave data *1* also consistently correlate with the experimental points from the paper by (Hasegawa et al., 2019), nearly crossing their midpoint *3*.

Thus, the model calculations of the thermal conductivity coefficient ε-Fe of iron in a highly defective shock-compressed state, carried out using the Wiedemann-Franz law and the theoretical value of the Lorentz number, satisfactorily agree with the static experiment.

Finally, let us consider algebraic calculations according to formulas (9) and (11) for ε-Fe at constant volume in the region of extrapolation to higher pressures. For example, we will set the specific volume in these formulas to $V = \text{const} = V_i = 4.282$ cm^3/mol and construct isochores (9) and (11) in the temperature range $T = 1000$–6000 K. According to the equation of state for ε-Fe constructed above, the range of pressures $P_i = P(V_i, T)$ will be 256–297 GPa, which includes the pressure at the boundaries of the Earth's inner core. The resulting graphs $\rho = \rho(T, V_i)$ and $k = k(T, V_i)$ are indicated with *1* in Figs. 10a and 10b, respectively.

Figures 10a and 10b also show the results of the fundamental calculations (Xu et al., 2018) of the temperature dependence $\rho = \rho(T, V_i)$ and $k = k(T, V_i)$ based on density functional theory method *2*. As can be seen, graphs *1* and *2* are in reasonable agreement with each other both qualitatively and quantitatively. The best fit between *1* and *2* is observed in a temperature range of 4000–6000, where the differences do not exceed 5% for $\rho = \rho(T, V_i)$ and 20% for $k = k(T, V_i)$.

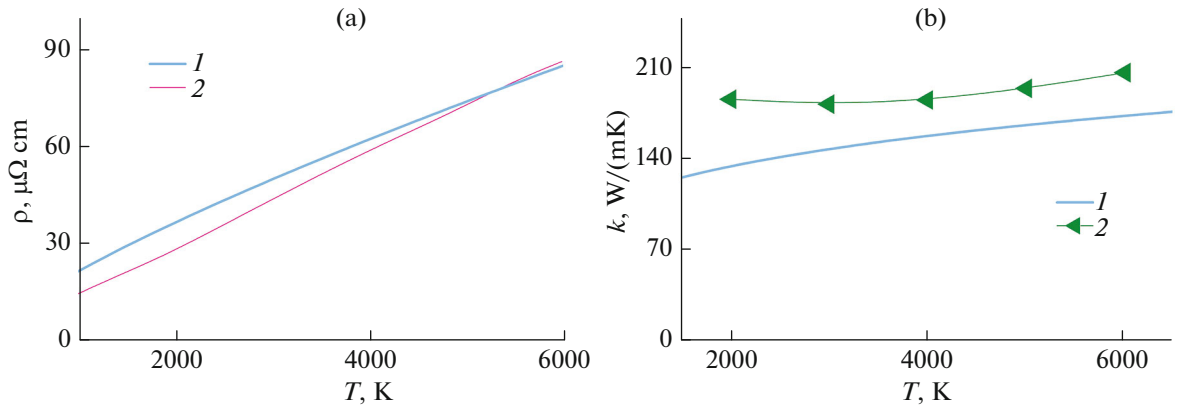

Fig. 10. Extrapolation of the dependences of the electrical resistivity ρ (a) and the thermal conductivity k (b) on the temperature T to the 300 GPa pressure region. a: *1*—isochore (9), *2*—the calculated temperature dependence of the ε-Fe electrical resistivity, given the saturation effect (Xu et al., 2018); b: *1*—isochore (11), *2*—the calculated temperature dependence of the ε-Fe thermal conductivity coefficient, given the saturation effect (Xu et al., 2018).

CONCLUSIONS

The electrical resistance of iron samples with a hexagonal close–packed lattice (ε-Fe) was measured under specific loading conditions consisting of a stepwise–cyclic compression phase followed by a phase of gradual pressure reduction. The measurements were made in the region of the iron phase diagram at pressures of ≈20–70 GPa and temperatures of ≈750–950 K.

The value of complicating effects during the measurement of the electrical resistance of shock compressed iron samples, caused by the conductivity of the insulating medium, the skin effect, and the heating of the sample by the surrounding hot insulator, was considered.

The equations of state of ε-Fe of iron have been developed, which, together with the determining ratio for the volume-temperature dependence of the resistivity, allow modeling an electrophysical shock-wave experiment, moving from the resistance of samples to specific values and determining the parameters characterizing the volume-temperature dependence of the resistivity of ε-Fe of iron during its stepwise shock loading and subsequent unloading

The volume–temperature dependences of the ε-Fe electrical resistivity under high static and dynamic pressures were compared. It was shown that in a pressure range of 20–70 GPa, the shock wave electrophysical data exceed the experimental literature static data by 10–30 μΩ cm.

The difference in the electrical properties of ε-Fe iron under static and shock compression and the similarity of the electrical properties of shock-compressed ε-Fe iron with the electrical properties of statically compressed and heated silicon iron have been established.

Calculations of the volume–temperature dependence of the ε-Fe thermal conductivity coefficient based on the Wiedemann–Franz law were performed to describe the thermal properties of ε-Fe at high dynamic pressures, and the calculated values of the thermal properties of shock compressed ε-Fe were compared with literature data at high static pressures. It was shown that in a pressure range of 20–50 GPa, the pressure dependence of the thermal conductivity coefficient along the room isotherm is in satisfactory agreement with the static experiment. It was also shown that the calculated values of the thermal conductivity coefficient in a temperature range of 1200–1500 K consistently correlate with the experimental points along the 53 GPa isobar.

Extrapolation of the found volume–temperature dependences of the ε-Fe electrical resistance and thermal conductivity to the 300 GPa pressure region is in reasonable agreement with the literature theoretical results on electrical and thermal conductivity of iron.

FUNDING

This study was financially supported by the Ministry of Science and Higher Education of the Russian Federation (Agreement with the Joint Institute for High Temperatures of the Russian Academy of Sciences No. 075-15-2020-785 dated September 23, 2020).

CONFLICT OF INTEREST

The authors declare that they have no conflicts of interest.

REFERENCES

Adadurov, G.A., Experimental study of chemical processes under dynamic compression conditions, *Russ. Chem. Rev.*, 1986, vol. 55, no. 4, pp. 282–296.

Basu, A., Field, M.R., McCulloch, D.G., and Boehler, R., New measurement of melting and thermal conductivity of iron close to outer core conditions, *Geosci. Front.,* 2020, vol. 11, no. 2, pp. 565–568.

Bi, Y., Tan, H., and Jing, F., Electrical conductivity of iron under shock compression up to 200 GPa, *J. Phys.: Condens. Matter*, 2002, vol.14, no. 44, pp. 10849–10854.

Brown, J.M., Fritz, J.N., and Hixson, R.S., Hugoniot data for iron, *J. Appl. Phys.*, 2000, vol. 88, no. 9, pp. 5496–5498.

Dewaele, A., Loubeyre, P., Occelli, F., Mezouar, M., Dorogokupets, P.I., and Torrent, M., Quasihydrostatic equation of state of iron above 2 Mbar, *Phys. Rev. Lett.*, 2006, vol. 97, Article ID 215504.

Golyshev, A.A. and Molodets, A.M., Electrical resistivity of plastic insulation at megabar shock pressures, *Combust., Explos., Shock Waves,* 2013, vol. 49, no. 2, pp. 219–224.

Gomi, H., Ohta, K., Hirose, K., Labrosse, S., Caracas, R., Verstraete, M.J., and Hernlund, J.W., The high conductivity of iron and thermal evolution of the Earth's core, *Phys.Earth Planet. Inter.*, 2013, vol. 224, pp. 88–103.

Grant, S.C., Ao, T., Seagle, C.T., Porwitzky, A.J., Davis, J.-P., Cochrane, K.R., Dolan, D.H., Lin, J.-F., Ditmire, T., and Bernstein, A.C., Equation of state measurements on iron near the melting curve at planetary core conditions by shock and ramp compressions, *J. Geophys. Res.: Solid Earth*, 2021, vol. 126, no. 3, Article ID e2020-JB020008.

Hasegawa, A., Yagi, T., and Ohta, K., Combination of pulsed light heating thermoreflectance and laserheated diamond anvil cell for in-situ high pressure-temperature thermal diffusivity measurements, *Rev. Sci. Instrum.*, 2019, vol. 90, no. 7, Article ID 074901.

Hirose, K., Wood, B., and Vočadlo, L., Light elements in the Earth's core, *Nat. Rev. Earth Environ.*, 2021, vol. 2, no. 9, pp. 645–658.

Johnson, P.C., Stein, B.A., and Davis, R.S., Temperature dependence of the shock induced transformation in iron, *J. Appl. Phys.*, 1962, vol. 33, no. 2, pp. 557–560.

Keeler, R.N. and Mitchel, A.C., Electrical conductivity, demagnetization, and the high-pressure phase transition in shock-compressed Iron, *Solid State Commun.,* 1969, vol. 7, no. 2, pp. 271–274.

Kerley, G.I., *Multiphase Equation of State for Iron*, technical rep. SAND93-0027, Albuquerque: Sandia 613 National Laboratories, 1993.

Kim, V.V. and Molodets, A.M., *Programma dlya rascheta volnovykh vzaimodeistvii i termodinamicheskogo sostoyaniya mnogosloinykh mishenei pri odnomernom udarnom nagruzhenii STAG* (Program for Calculation of Wave Interactions and Thermodynamic State of Multilayer Targets under One–Dimensional Shock Loading STAG). Certificate of state registration of the computer program no. 2016616914. 22.06.2016.

Mao, H.K., Wu, Y., Chen, L.C., Shu, J.F., and Jephcoat, A.P., Static compression of iron to 300 GPa and $Fe_{0.8}Ni_{0.2}$ alloy to 260 GPa: Implications for compression of the core, *J. Geophys. Res.*, 1990, vol. 95, no. B13, pp. 21737–21742.

Molodets, A.M., Temperature dependence of the spall strength and equation of state for austenitic chromium–nickel steel 18-10, *Phys. Solid State*, 2015, vol. 57, no. 10, pp. 2045–2050.

Molodets, A.M., Equations of state muscovite at high pressures and high temperatures, *Izv., Phys. Solid Earth*, 2022, no. 1, pp. 117–126.

Molodets, A.M. and Golyshev, A.A., Volume-temperature dependence of electrical and thermophysical properties of α-iron under high pressures and temperatures, *Tech. Phys.*, 2021, vol. 66, no. 11, pp. 1247–1252.

Molodets, A.M., Shakhrai, D.V., Savinykh, A.S., Golyshev, A.A., and Kim, V.V., Equation of state of polytetrafluoroethylene for calculating shock compression parameters at megabar pressures, *Combust., Explos., Shock Waves,* 2013, vol. 49, no. 6, pp. 731–738.

Molodets, A.M., Shakhrai, D.V., and Golyshev, A.A., Semiempirical description of thermophysical properties of lithium deuteride at high pressures and temperatures, *High Temp.,* 2017, vol. 55, no. 4, pp. 510–514.

Molodets, A.M., Golyshev, A.A., Emel'yanov, A.N., and Kozlov, A.A., Magnetic transformations and polymorphic transition of ferromagnetic steels under shock-wave loading, *Tech. Phys.*, 2021, vol. 66, no. 6, pp. 755–759.

Nabatov, S.S., Dremin, A.N., Postnov, V.I., and Yakushev, V.V., Measurement of the electrical conductivity of sulfur under superhigh dynamic pressures, *JETP Lett.*, 1979, vol. 29, no. 7, pp. 369–372.

Ohta, K., Kuwayama, Y., Hirose, K., Shimizu, K., and Ohishi, Y., Experimental determination of the electrical resistivity of iron at Earth's core conditions, *Nature*, 2016, vol. 534, no. 7605, pp. 95–98.

Ohta, K., Nishihara, Y., Sato, Y., Hirose, K., Yagi T., Kawaguchi, S.I., Hirao, N., and Ohishi, Y., An experimental examination of thermal conductivity anisotropy in *hcp* iron, *Front. Earth Sci.,* 2018, vol. 6, Article ID 176.

Seagle, C.T., Cottrell, E., Fei, Y., Hummer, D.R., and Prakapenka, V.B., Electrical and thermal transport properties of iron and iron-silicon alloy at high pressure, *Geophys. Res. Lett.,* 2013, vol. 40, no. 20, pp. 5377–5381.

Vočadlo, L., Mineralogy of the Earth—the Earth's core: iron and iron alloys, Ch. 5 of *Mineral Physics, Treatise on Geophysics*, vol. 2, Price, G.D., Ed., Oxford: Elsevier, 2007, pp. 91–120.

Xu, J., Zhang, P., Haule, K., Minar, J., Wimmer, S., Ebert, H., and Cohen, R.E., Thermal conductivity and electrical resistivity of solid iron at Earth's core conditions from first principles, *Phys. Rev. Lett.*, 2018, vol. 121, no. 9, Article ID 096601.

Yang, F., Hu, X., and Fei, Y., *In situ* measurements of electrical resistivity of metals in a cubic multi-anvil apparatus by van der Pauw method, *Rev. Sci. Instrum.*, 2022, vol. 93, no. 5, Article ID 053902.

Zhang, Y., Hou, M., Liu, G., Zhang, Ch., Prakapenka, V.B., Greenberg, E., Fei, Y., Cohen, R.E., and Lin, J.F., Reconciliation of experiments and theory on transport properties of iron and the geodynamo, *Phys. Rev. Lett.*, 2020, vol. 125, no. 7, Article ID 078501.

Zhang, Y., Luo, K, Hou, M., Driscoll, P., Salke, N.P., Minar, J., Prakapenka, V.B., Greenberg, E., Hemley, R.J., Cohen, R.E., and Lin, J.F., Thermal conductivity of Fe-Si alloys and thermal stratification in Earth's core, *Proc. Natl. Acad. Sci. U. S. A.*, 2022, vol. 119, no. 1, Article ID e2119001119.

Zharkov, V.N., *Fizika zemnykh nedr* (Physics of the Earth's Interior), Moscow: Nauka i obrazovanie, 2012.